

# The superradiant phase is a finite size effect in two-photon processes

Fabrizio Ramírez,<sup>1</sup> David Villaseñor,<sup>2,\*</sup> Nahum Vázquez,<sup>1</sup> and Jorge G. Hirsch<sup>1,†</sup>

<sup>1</sup>*Instituto de Ciencias Nucleares, Universidad Nacional Autónoma de México,  
Apdo. Postal 70-543, C.P. 04510 Mexico City, Mexico*

<sup>2</sup>*CAMTP - Center for Applied Mathematics and Theoretical Physics,  
University of Maribor, Mladinska 3, SI-2000 Maribor, Slovenia, European Union*

Two-photon light–matter interactions exhibit distinctive features such as spectral collapse. The two-photon Dicke model has been reported to exhibit a superradiant phase which could be useful in quantum applications. Here we show that this superradiant phase is not a genuine thermodynamic phase but a finite-size effect. Combining analytical and numerical analyses, we demonstrate that the superradiant region shrinks with increasing system size and disappears in the thermodynamic limit, while spectral collapse remains. Our results clarify the nature of superradiant conditions in two-photon systems and constrain its realization in quantum platforms.

Understanding the interaction between light and matter is a central problem in quantum optics [1] and underpins a wide range of quantum technologies, including quantum metrology [2–6], simulation [7, 8], and communication [9–12]. Cavity and circuit quantum electrodynamics provide controlled settings in which collective atom–field effects emerge [9, 13], often leading to enhanced coherence and cooperative phenomena that have no single-particle counterpart.

Among the paradigmatic models describing collective light–matter interactions is the Dicke model [14–18], which captures the coupling between an ensemble of two-level systems (qubits) and a single bosonic mode. The Dicke model exhibits a well-established superradiant phase transition in the thermodynamic limit [19–23], characterized by macroscopic occupation of the field mode and collective atomic excitation. This transition has been extensively studied both theoretically [24–35] and experimentally [36–40] and forms a cornerstone of the understanding of collective quantum behavior.

Recent interest has shifted toward multiphoton light–matter interactions [41, 42], motivated by advances in experimental platforms such as trapped ions, superconducting circuits, Rydberg atoms, quantum dots, and quantum batteries [43–54]. In particular, two-photon processes, where atomic excitations are accompanied by the simultaneous creation or annihilation of two bosonic excitations, lead to qualitatively new physics [41, 42, 55–59]. The two-photon Rabi and Dicke models display rich spectral properties, including spectral collapse [60–63], in which discrete energy levels merge into a continuous band at a critical coupling strength. This phenomenon has no analogue in single-photon models.

The two-photon Dicke model [17, 60, 63–68] has attracted special attention because it has been reported to exhibit a superradiant phase [69, 70] based on analytical treatments using Holstein–Primakoff and squeezed-state mean-field approaches. This superradiant phase has been found even in the presence of dissipation [71, 72]. It has motivated proposals for exploiting two-photon interactions in quantum technologies expected to operate under

superradiant conditions [53, 54, 73]. However, the nature of this superradiant phase and its stability in the thermodynamic limit have remained insufficiently scrutinized.

In this work, we show that the superradiant phase of the two-photon Dicke model is not a genuine thermodynamic phase, but rather a finite-size effect. By combining analytical mean-field results with numerical simulations, we demonstrate that the region associated with superradiant behavior systematically shrinks as the system size increases and vanishes entirely in the thermodynamic limit. Crucially, we compare two independent classical limits, one based on squeezed vacuum states and one based on Glauber coherent states, and show that only the latter yields physically meaningful stationary solutions as the system size diverges. In contrast, the stationary solutions of the first classical limit related to superradiance become complex and unphysical in the thermodynamic limit.

Our results clarify the relationship between superradiance and spectral collapse in two-photon light–matter systems. We find that spectral collapse survives the thermodynamic limit and admits a clear interpretation in bosonic phase space, whereas superradiance does not. This distinction resolves an apparent inconsistency in previous analyses and imposes fundamental constraints on the realization of superradiant behavior in two-photon platforms.

*Two-photon Dicke model*— The two-photon Dicke model describes the collective interaction between  $\mathcal{N}$  two-level systems and a single-mode bosonic field of frequency  $\omega$ , where atomic excitations are accompanied by the simultaneous creation or annihilation of two bosonic quanta. Setting  $\hbar = 1$ , the Hamiltonian reads

$$\hat{H}_D = \omega \hat{a}^\dagger \hat{a} + \omega_0 \hat{J}_z + \frac{\gamma}{\mathcal{N}} \left( \hat{a}^{\dagger 2} + \hat{a}^2 \right) \left( \hat{J}_+ + \hat{J}_- \right), \quad (1)$$

where  $\hat{a}^\dagger$  and  $\hat{a}$  are the creation and annihilation operators satisfying  $[\hat{a}, \hat{a}^\dagger] = \hat{\mathbb{I}}$ . The collective atomic operators  $\hat{J}_z$  and  $\hat{J}_\pm = \hat{J}_x \pm i\hat{J}_y$  obey the standard angular-momentum commutation relations  $[\hat{J}_z, \hat{J}_\pm] = \pm \hat{J}_\pm$  and  $[\hat{J}_+, \hat{J}_-] = 2\hat{J}_z$ , and are defined as  $\hat{J}_{x,y,z} =$

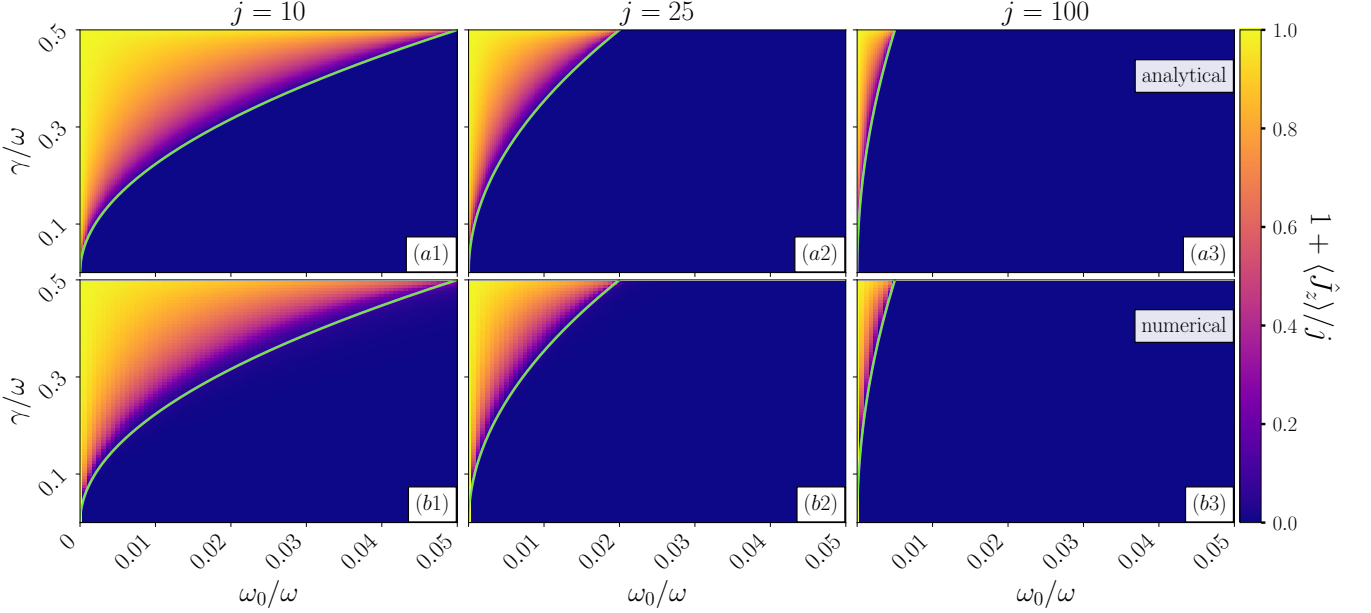


FIG. 1. (a1)-(a3) Phase diagrams of the normalized atomic excitation  $1 + \langle \hat{J}_z \rangle / j$  [Eq. (7)] as a function of the scaled atomic frequency  $\omega_0 / \omega$  and the scaled coupling parameter  $\gamma / \omega$ . The color scale represents the numerical value of the last observable. The green solid line represents the scaled critical coupling  $\gamma_c / \omega = \sqrt{\omega_0 j / (2\omega)}$ . (b1)-(b3) Numerical implementations of panels (a1)-(a3). Each column identifies a different system size: (a1)-(b1)  $j = 10$ , (a2)-(b2)  $j = 25$ , and (a3)-(b3)  $j = 100$ .

$(1/2) \sum_{k=1}^N \hat{\sigma}_{x,y,z}^k$ . In the above Hamiltonian,  $\omega_0$  denotes the atomic transition frequency, and  $\gamma$  is the atom–field coupling strength. The coupling is bounded by the critical value  $\gamma_{sc} = \omega/2$ , at which spectral collapse occurs [60–62].

The Hamiltonian  $\hat{H}_D$  possesses a discrete parity symmetry,  $[\hat{H}_D, \hat{\Pi}] = 0$ , where the parity operator is defined as  $\hat{\Pi} = \exp(i\pi\hat{\Lambda})$ , with  $\hat{\Lambda} = \hat{a}^\dagger\hat{a}/2 + \hat{J}_z + j\hat{I}$ . This symmetry partitions the Hilbert space into four invariant subspaces labeled by the eigenvalues  $p = \pm 1, \pm i$  of  $\hat{\Pi}$ , corresponding to the simultaneous transformations  $\hat{a} \rightarrow i\hat{a}$  and  $\hat{J}_x \rightarrow -\hat{J}_x$ .

In addition, the total collective spin  $\hat{\mathbf{J}}^2 = \hat{J}_x^2 + \hat{J}_y^2 + \hat{J}_z^2$  is conserved,  $[\hat{H}_D, \hat{\mathbf{J}}^2] = 0$ , allowing the Hilbert space to be decomposed into sectors characterized by the eigenvalue  $j(j+1)$ . Throughout this work, we focus on the fully symmetric subspace with  $j = N/2$ , which governs the collective behavior of the model and is relevant for the thermodynamic limit.

*Ground state, classical limit, and superradiant phase*—The ground state of the two-photon Dicke model can be obtained at the mean field level by applying a Holstein–Primakoff transformation to the collective spin operators, followed by a Bogoliubov transformation of the bosonic mode. This procedure yields a squeezed-vacuum ground state of the form [69]

$$|E_0\rangle = |r_b\rangle = e^{(r_b^* \hat{a}^2 - r_b \hat{a}^{\dagger 2})/2} |0\rangle, \quad (2)$$

where  $r_b \in \mathbb{R}$  is the squeezing parameter and  $|0\rangle$  denotes

the bosonic vacuum. Minimization of the ground-state energy  $E_0$  identifies two regimes separated by the critical coupling  $\gamma_c = \sqrt{\omega_0 j / 2}$ . For  $\gamma < \gamma_c$  the system is in a normal phase (NP), while for  $\gamma > \gamma_c$  a superradiant phase (SP) emerges. Details of this derivation are given in Ref. [69] and in the Supplemental Material [74].

To establish a classical description of the model, we introduce a similar mean-field approximation based on the tensor product  $|\mathbf{x}\rangle \equiv |\xi\rangle \otimes |\beta\rangle$ , where  $|\xi\rangle = e^{(\xi^* \hat{a}^2 - \xi \hat{a}^{\dagger 2})/2} |0\rangle$  is a squeezed vacuum state with  $\xi = r e^{i\theta}$ , and  $|\beta\rangle = (1 + |\beta|^2)^{-j/2} e^{\beta \hat{J}_+} |j, -j\rangle$  is a Bloch coherent state for the collective spin. The associated classical Hamiltonian is defined as

$$\begin{aligned} h_D(\mathbf{x}) &= \frac{1}{j} \langle \mathbf{x} | \hat{H}_D | \mathbf{x} \rangle \quad (3) \\ &= \Omega(\mathbf{x}) - 2\gamma q Q \sqrt{\left(\frac{1}{2j} + \frac{q^2 + p^2}{4}\right) \left(1 - \frac{Q^2 + P^2}{4}\right)}, \end{aligned}$$

with  $\Omega(\mathbf{x}) = (\omega/2)(q^2 + p^2) + (\omega_0/2)(Q^2 + P^2) - \omega_0$ . Here,  $\mathbf{x} = (q, p; Q, P)$  are canonical variables describing the bosonic and atomic degrees of freedom, and the classical energy has been scaled by the system size,  $h_D(\mathbf{x}) = E/j$ . The atomic variables  $(Q, P)$  are related to the Bloch parameter  $\beta = (Q + iP)/\sqrt{4 - Q^2 - P^2}$ , while the bosonic variables  $(q, p)$  are introduced via

$$(q, p) = \sqrt{\frac{2}{j}} \sinh(r) [\cos(\theta), \sin(\theta)]. \quad (4)$$

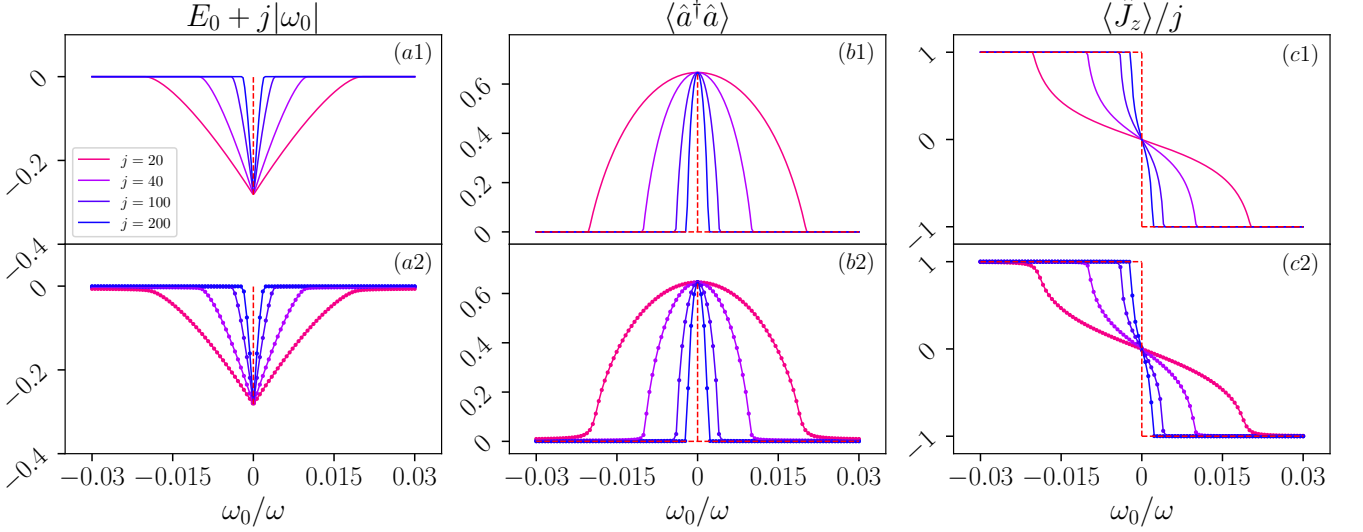


FIG. 2. Projections of (a1) displaced ground-state energy  $E_0 + j|\omega_0|$  [Eq. (5)], (b1) number of photons  $\langle \hat{a}^\dagger \hat{a} \rangle$  [Eq. (6)], and (c1) atomic operator  $\langle \hat{J}_z \rangle/j$  [Eq. (7)], as a function of the scaled atomic frequency  $\omega_0/\omega$ . Each color identifies a different system size  $j = 20, 40, 100, 200$ . The red dashed line represents the thermodynamic limit  $j \rightarrow \infty$ . (a2)-(c2) Numerical implementations of panels (a1)-(c1). The coupling parameter is  $\gamma/\omega = 0.45$ .

The stationary points  $\mathbf{x}_m$  of the classical Hamiltonian are obtained from Hamilton's equations of motion. Using these extrema, we can obtain analytical expressions [74] for the ground-state energy,

$$E_0 = j h_D(\mathbf{x}_m) = \langle \mathbf{x}_m | \hat{H}_D | \mathbf{x}_m \rangle \quad (5)$$

$$= - \begin{cases} j|\omega_0| & \text{for (NP)} \\ \frac{\omega}{2} \left( 1 - \sqrt{\left( 1 - \frac{4\gamma^2}{\omega^2} \right) \left( 1 - \frac{j^2\omega_0^2}{\gamma^2} \right)} \right) & \text{for (SP)} \end{cases}$$

the number of photons

$$\langle \mathbf{x}_m | \hat{a}^\dagger \hat{a} | \mathbf{x}_m \rangle = \begin{cases} 0 & \text{for (NP)} \\ \frac{1}{2} \left( \sqrt{\frac{1 - \frac{j^2\omega_0^2}{\gamma^2}}{1 - \frac{4\gamma^2}{\omega^2}}} - 1 \right) & \text{for (SP)} \end{cases}, \quad (6)$$

and the atomic inversion,

$$\frac{\langle \mathbf{x}_m | \hat{J}_z | \mathbf{x}_m \rangle}{j} = - \begin{cases} \text{sgn}(\omega_0) & \text{for (NP)} \\ \frac{j\omega_0\omega}{2\gamma^2} \sqrt{\frac{1 - \frac{4\gamma^2}{\omega^2}}{1 - \frac{j^2\omega_0^2}{\gamma^2}}} & \text{for (SP)} \end{cases}. \quad (7)$$

We emphasize that the ground-state energy obtained from this mean-field construction coincides with that derived from the Holstein–Primakoff and Bogoliubov transformations [69]. These expressions provide the starting point for analyzing the fate of the superradiant phase as the system size is increased and the thermodynamic limit is approached.

*Thermodynamic limit and disappearance of the superradiant phase*— The thermodynamic limit of the two-photon Dicke model is defined by  $\mathcal{N} \rightarrow \infty$ , or equivalently, when  $j = \mathcal{N}/2 \rightarrow \infty$ . In this limit, collective

atom–field systems are expected to display macroscopic behavior and well-defined phase transitions. The analytical expressions derived in Eqs. (5)–(7) allow us to track explicitly how the ground-state properties evolve with increasing system size.

Figures 1(a1)–1(a3) present phase diagrams of the normalized atomic excitation  $1 + \langle \hat{J}_z \rangle/j$  [Eq. (7)] as functions of the scaled atomic frequency  $\omega_0/\omega$  and the scaled coupling strength  $\gamma/\omega$  for increasing values of  $j$ . For finite system sizes, two distinct regions corresponding to the normal and superradiant phases are separated by the critical coupling  $\gamma_c = \sqrt{\omega\omega_0j/2}$ . However, as the system size increases, the superradiant region shrinks progressively. In the limit  $j \rightarrow \infty$ , this region collapses entirely, leaving only the normal phase. The numerical results [Figs. 1(b1)–1(b3)] are in complete agreement with the analytical predictions. We present similar phase diagrams for the number of photons  $\langle \hat{a}^\dagger \hat{a} \rangle$  [Eq. (6)] and the ground-state energy  $E_0$  [Eq. (5)] in the Supplemental Material [74].

The previous behavior is further illustrated in Figs. 2(a1)–2(c1), which show projections of the ground-state energy, photon number, and atomic inversion as functions of  $\omega_0/\omega$  at fixed coupling  $\gamma/\omega < 1/2$ , respectively. For finite  $j$ , these observables display the smooth crossover associated with the analytically defined superradiant phase. As  $j$  increases, the crossover region narrows and converges to a singular structure in the thermodynamic limit. At  $\omega_0 = 0$ , the ground-state energy develops a finite discontinuity, the photon number approaches a delta-like peak, and the atomic inversion becomes a step function. These limiting behaviors are incompat-

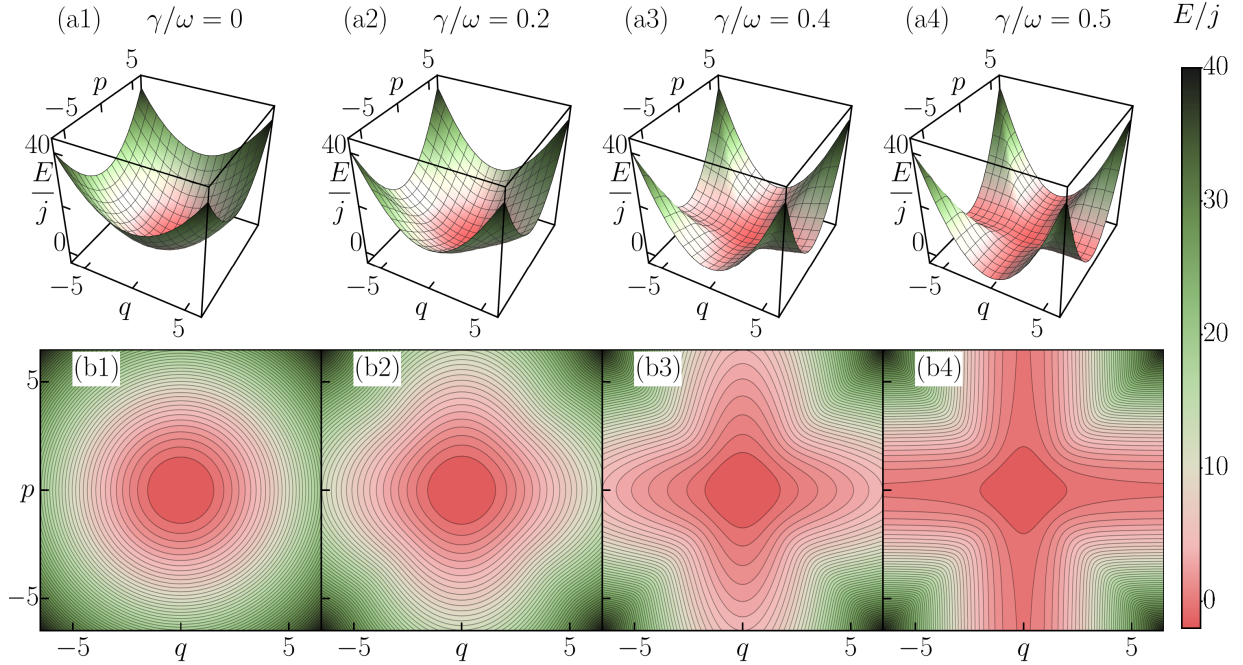


FIG. 3. (a1)-(a4) Energy surface  $h_D(q,p)$  in Eq. (9) as a function of the bosonic coordinates  $(q,p)$  for increasing coupling parameter  $\gamma/\omega = 0.1, 0.2, 0.4, 0.5$ , scaled by the field frequency  $\omega$ . (b1)-(b4) Orthogonal projections of panels (a1)-(a4) over the bosonic plane  $(q,p)$ . The color scale shows values of the scaled classical energy  $E/j$  that begins at the scaled ground-state energy  $E_0/j = -|\omega_0|$ . System parameters:  $\omega = 1$  and  $\omega_0 = 2\omega$ .

ible with the existence of a stable superradiant phase. The numerical results [Figs. 2(a2)-2(c2)] again show full agreement with the analytical results.

The disappearance of the superradiant phase can be understood directly from the analytical expressions. In Eqs. (5)-(7), the stationary solutions associated with the superradiant phase require  $j^2\omega_0^2 < \gamma^2$ , a condition that cannot be satisfied as  $j \rightarrow \infty$  at fixed  $\gamma$  and  $\omega_0$ . Consequently, the corresponding mean-field extrema become unphysical in the thermodynamic limit, signaling the breakdown of the superradiant solutions [74].

From the previous evidence, we conclude that the superradiant phase does not survive the thermodynamic limit in the two-photon Dicke model. The phase identified at finite system sizes represents a finite-size crossover rather than a genuine quantum phase transition. This result sets the stage for the alternative classical description discussed below, which correctly captures the thermodynamic behavior and the onset of spectral collapse.

*Spectral collapse in bosonic phase space*— The disappearance of the superradiant phase in the thermodynamic limit calls for an alternative classical description of the two-photon Dicke model. We therefore consider a second mean-field construction based on Glauber coherent states for the bosonic mode, which provides a natural consistent classical limit as  $j \rightarrow \infty$ .

Specifically, we introduce the product state  $|\mathbf{y}\rangle \equiv |\alpha\rangle \otimes |\beta\rangle$ , where  $|\alpha\rangle = e^{-|\alpha|^2/2} e^{\alpha \hat{a}^\dagger} |0\rangle$  is a Glauber co-

herent state and  $|\beta\rangle$  is the Bloch coherent state used previously for the collective spin. The associated classical Hamiltonian is defined as

$$h_D(\mathbf{y}) = \frac{1}{j} \langle \mathbf{y} | \hat{H}_D | \mathbf{y} \rangle \quad (8)$$

$$= \Omega(\mathbf{y}) + \gamma (q^2 - p^2) Q \sqrt{1 - \frac{Q^2 + P^2}{4}},$$

with  $\Omega(\mathbf{y}) = (\omega/2)(q^2 + p^2) + (\omega_0/2)(Q^2 + P^2) - \omega_0$ . Here,  $h_D(\mathbf{y}) = E/j$ ,  $\mathbf{y} = (q, p; Q, P)$  denotes the classical phase-space variables, and the bosonic coordinates are defined through the Glauber parameter  $\alpha = \sqrt{j/2}(q + ip)$ .

The stationary points  $\mathbf{y}_m$  of the classical Hamiltonian are obtained from Hamilton's equations. Among these solutions, there is only a single real stationary point  $\mathbf{y}_0$ , which reproduces the ground-state energy of the normal phase  $E_0 = -j\omega_0$ . The remaining stationary solutions  $\mathbf{y}_\pm$  are complex and therefore do not correspond to physical classical states. Notably, in the thermodynamic limit  $j \rightarrow \infty$ , the stationary solutions  $\mathbf{x}_\pm$  associated with the superradiant phase in the squeezed-state construction continuously evolve into these complex solutions  $\mathbf{y}_\pm$ . This correspondence provides direct mathematical evidence that the superradiant phase has no physical meaning in the thermodynamic limit [74].

Having identified the coherent-state construction as the appropriate classical limit, we now use it to characterize spectral collapse in phase space. Eliminating the

atomic variables by solving  $\partial_Q h_D(\mathbf{y}) = \partial_P h_D(\mathbf{y}) = 0$ , we obtain stationary solutions  $Q_m = Q_m(q, p)$  and  $P_m = 0$ , leading to an effective energy surface projected onto the bosonic variables

$$h_D(q, p) = h_D(q, p; Q_m, 0) \quad (9)$$

$$= \frac{\omega}{2} (q^2 + p^2) - \omega_0 \sqrt{1 + \frac{\gamma^2}{\omega_0^2} (q^2 - p^2)^2}.$$

Figure 3 shows the resulting energy surface for increasing values of the scaled coupling  $\gamma/\omega$  at fixed resonance  $\omega_0 = 2\omega$ . For weak coupling, the surface is bounded and displays a single global minimum, characteristic of the normal phase. As  $\gamma/\omega$  approaches the collapse value  $\gamma_{sc}/\omega = 1/2$ , the surface progressively flattens and eventually becomes unbounded, developing extended regions at the ground-state energy across both  $q$  and  $p$  axes [Figs. 3(a4) and 3(b4)]. This transition from a bounded to an unbounded energy landscape provides a clear classical signature of spectral collapse in bosonic phase space.

*Conclusion*— We demonstrated that the superradiant phase of the two-photon Dicke model is not a genuine thermodynamic phase but a finite-size effect. Although a superradiant region emerges at finite system size, it collapses systematically as the number of atoms increases and disappears in the thermodynamic limit. In this limit, the stationary solutions associated with superradiance become unphysical, while the coherent-state classical limit admits only the normal phase and correctly captures the onset of spectral collapse.

Our results demonstrate that superradiance and spectral collapse are fundamentally distinct phenomena in two-photon light-matter systems. In particular, spectral collapse survives the thermodynamic limit, whereas superradiance does not. This resolves an apparent contradiction in previous analyses based on squeezed-state mean-field treatments and places strong constraints on the realization of superradiant behavior in two-photon platforms. Whether dissipation [71, 72] can stabilize a genuine superradiant phase remains an open and non-trivial question.

*Acknowledgments*— We acknowledge the support of the Computation Center - ICN, in particular to Enrique Palacios, Luciano Díaz, and Eduardo Murrieta. F.R., N.V., and J.G.H acknowledge partial financial support from the DGAPA-UNAM Projects No. IN109523 and IN101526. D.V. acknowledges financial support from the Slovenian Research and Innovation Agency (ARIS) under Grants No. J1-4387 and No. P1-0306.

- [2] Michael A. Taylor and Warwick P. Bowen, “Quantum metrology and its application in biology,” *Phys. Rep.* **615**, 1–59 (2016).
- [3] C. L. Degen, F. Reinhard, and P. Cappellaro, “Quantum sensing,” *Rev. Mod. Phys.* **89**, 035002 (2017).
- [4] Lukas J. Fiderer and Daniel Braun, “Quantum metrology with quantum-chaotic sensors,” *Nature Commun.* **9**, 1351 (2018).
- [5] Scott E. Crawford, Roman A. Shugayev, Hari P. Paudel, Ping Lu, Madhava Syamlal, Paul R. Ohodnicki, Benjamin Chorpening, Randall Gentry, and Yuhua Duan, “Quantum sensing for energy applications: Review and perspective,” *Adv. Quantum Technol.* **4**, 2100049 (2021).
- [6] Victor Montenegro, Chiranjib Mukhopadhyay, Rozhin Yousefjani, Saubhik Sarkar, Utkarsh Mishra, Matteo G.A. Paris, and Abolfazl Bayat, “Review: Quantum metrology and sensing with many-body systems,” *Phys. Rep.* **1134**, 1–62 (2025).
- [7] Seth Lloyd, “Universal quantum simulators,” *Science* **273**, 1073–1078 (1996).
- [8] I. M. Georgescu, S. Ashhab, and Franco Nori, “Quantum simulation,” *Rev. Mod. Phys.* **86**, 153–185 (2014).
- [9] Anton Zeilinger, “Experiment and the foundations of quantum physics,” *Rev. Mod. Phys.* **71**, S288–S297 (1999).
- [10] Nicolas Gisin and Rob Thew, “Quantum communication,” *Nature Photonics* **1**, 165–171 (2007).
- [11] Brian Swingle, Gregory Bentsen, Monika Schleier-Smith, and Patrick Hayden, “Measuring the scrambling of quantum information,” *Phys. Rev. A* **94**, 040302 (2016).
- [12] K. A. Landsman, C. Figgatt, T. Schuster, N. M. Linke, B. Yoshida, N. Y. Yao, and C. Monroe, “Verified quantum information scrambling,” *Nature* **567**, 61–65 (2019).
- [13] Jonathan P. Dowling and Gerard J. Milburn, “Quantum technology: the second quantum revolution,” *Phil. Trans. Roy. Soc. A* **361**, 1655–1674 (2003).
- [14] R. H. Dicke, “Coherence in spontaneous radiation processes,” *Phys. Rev.* **93**, 99 (1954).
- [15] Peter Kirton, Mor M. Roses, Jonathan Keeling, and Emanuele G. Dalla Torre, “Introduction to the Dicke model: From equilibrium to nonequilibrium, and vice versa,” *Adv. Quantum Technol.* **2**, 1800043 (2019).
- [16] Mor M. Roses and Emanuele G. Dalla Torre, “Dicke model,” *PLoS ONE* **15**, 1–8 (2020).
- [17] Jonas Larson and Themistoklis Mavrogordatos, *The Jaynes–Cummings Model and Its Descendants*, 2053–2563 (IOP Publishing, 2021).
- [18] David Villaseñor, Saúl Pilatowsky-Cameo, Jorge Chávez-Carlos, Miguel A. Bastarrachea-Magnani, Sergio Lerma-Hernández, Lea F. Santos, and Jorge G. Hirsch, “Classical and quantum properties of the spin-boson Dicke model: Chaos, localization, and scarring,” (2024), arXiv:2405.20381 [quant-ph].
- [19] Clive Emery and Tobias Brandes, “Chaos and the quantum phase transition in the Dicke model,” *Phys. Rev. E* **67**, 066203 (2003).
- [20] Clive Emery and Tobias Brandes, “Quantum chaos triggered by precursors of a quantum phase transition: The Dicke model,” *Phys. Rev. Lett.* **90**, 044101 (2003).
- [21] Neill Lambert, Clive Emery, and Tobias Brandes, “Entanglement and the phase transition in single-mode superradiance,” *Phys. Rev. Lett.* **92**, 073602 (2004).
- [22] Tobias Brandes, “Coherent and collective quantum optical effects in mesoscopic systems,” *Phys. Rep.* **408**, 315–

\* d.v.pcf.cu@gmail.com

† hirsch@nucleares.unam.mx

[1] Marlan O. Scully and M. Suhail Zubairy, *Quantum optics* (Cambridge University Press, Cambridge, 1997).

474 (2005).

[23] Tobias Brandes, “Excited-state quantum phase transitions in Dicke superradiance models,” *Phys. Rev. E* **88**, 032133 (2013).

[24] Nicholas E. Rehler and Joseph H. Eberly, “Superradiance,” *Phys. Rev. A* **3**, 1735–1751 (1971).

[25] R. Bonifacio, P. Schwendimann, and Fritz Haake, “Quantum statistical theory of superradiance. I,” *Phys. Rev. A* **4**, 302–313 (1971).

[26] J. C. MacGillivray and M. S. Feld, “Theory of superradiance in an extended, optically thick medium,” *Phys. Rev. A* **14**, 1169–1189 (1976).

[27] Michel Gross and Serge Haroche, “Superradiance: An essay on the theory of collective spontaneous emission,” *Phys. Rep.* **93**, 301–396 (1982).

[28] R. T. Sutherland and F. Robicheaux, “Superradiance in inverted multilevel atomic clouds,” *Phys. Rev. A* **95**, 033839 (2017).

[29] Stuart J. Masson, Igor Ferrier-Barbut, Luis A. Orozco, Antoine Browaeys, and Ana Asenjo-Garcia, “Many-body signatures of collective decay in atomic chains,” *Phys. Rev. Lett.* **125**, 263601 (2020).

[30] Stuart J. Masson and Ana Asenjo-Garcia, “Universality of Dicke superradiance in arrays of quantum emitters,” *Nature Communications* **13**, 2285 (2022).

[31] Eric Sierra, Stuart J. Masson, and Ana Asenjo-Garcia, “Dicke superradiance in ordered lattices: Dimensionality matters,” *Phys. Rev. Res.* **4**, 023207 (2022).

[32] A. Piñeiro Orioli, J. K. Thompson, and A. M. Rey, “Emergent dark states from superradiant dynamics in multilevel atoms in a cavity,” *Phys. Rev. X* **12**, 011054 (2022).

[33] Silvia Cardenas-Lopez, Stuart J. Masson, Zoe Zager, and Ana Asenjo-Garcia, “Many-body superradiance and dynamical mirror symmetry breaking in waveguide QED,” *Phys. Rev. Lett.* **131**, 033605 (2023).

[34] Stuart J. Masson, Jacob P. Covey, Sebastian Will, and Ana Asenjo-Garcia, “Dicke superradiance in ordered arrays of multilevel atoms,” *PRX Quantum* **5**, 010344 (2024).

[35] P. Rosario, L. O. R. Solak, A. Cidrim, R. Bachelard, and J. Schachenmayer, “Unraveling Dicke superradiant decay with separable coherent spin states,” *Phys. Rev. Lett.* **135**, 133602 (2025).

[36] N. Skribanowitz, I. P. Herman, J. C. MacGillivray, and M. S. Feld, “Observation of Dicke superradiance in optically pumped HF gas,” *Phys. Rev. Lett.* **30**, 309–312 (1973).

[37] J. M. Raimond, P. Goy, M. Gross, C. Fabre, and S. Haroche, “Collective absorption of blackbody radiation by Rydberg atoms in a cavity: An experiment on Bose statistics and Brownian motion,” *Phys. Rev. Lett.* **49**, 117–120 (1982).

[38] S. Inouye, A. P. Chikkatur, D. M. Stamper-Kurn, J. Stenger, D. E. Pritchard, and W. Ketterle, “Superradiant Rayleigh scattering from a Bose-Einstein condensate,” *Science* **285**, 571–574 (1999).

[39] S. Slama, S. Bux, G. Krenz, C. Zimmermann, and Ph. W. Courteille, “Superradiant Rayleigh scattering and collective atomic recoil lasing in a ring cavity,” *Phys. Rev. Lett.* **98**, 053603 (2007).

[40] Michael Scheibner, Thomas Schmidt, Lukas Worschel, Alfred Forchel, Gerd Bacher, Thorsten Passow, and Detlef Hommel, “Superradiance of quantum dots,” *Nat. Phys.* **3**, 106–110 (2007).

[41] C. F. Lo, K. L. Liu, and K. M. Ng, “The multiquantum Jaynes-Cummings model with the counter-rotating terms,” *Europhys. Lett.* **42**, 1 (1998).

[42] Daniel Braak, “The  $k$ -photon quantum Rabi model,” in *Mathematical Foundations for Post-Quantum Cryptography: Crypto-Math CREST*, edited by Tsuyoshi Takagi, Masato Wakayama, Noboru Kunihiro, Keisuke Tanaka, Kazufumi Kimoto, and Momonari Kudo (Springer Nature Singapore, Singapore, 2026) pp. 75–87.

[43] M. M. T. Loy, “Two-photon adiabatic inversion,” *Phys. Rev. Lett.* **41**, 473–476 (1978).

[44] H. Schlemmer, D. Frölich, and H. Welling, “Two-photon amplification on cascade-transitions,” *Opt. Commun.* **32**, 141–144 (1980).

[45] B. Nikolaus, D. Z. Zhang, and P. E. Toschek, “Two-photon laser,” *Phys. Rev. Lett.* **47**, 171–173 (1981).

[46] M. Brune, J. M. Raimond, and S. Haroche, “Theory of the Rydberg-atom two-photon micromaser,” *Phys. Rev. A* **35**, 154–163 (1987).

[47] M. Brune, J. M. Raimond, P. Goy, L. Davidovich, and S. Haroche, “Realization of a two-photon maser oscillator,” *Phys. Rev. Lett.* **59**, 1899–1902 (1987).

[48] M. Brune, J. M. Raimond, P. Goy, L. Davidovich, and S. Haroche, “The two-photon Rydberg atom micro-maser,” *IEEE J. Quantum Electronics* **24**, 1323–1330 (1988).

[49] Daniel J. Gauthier, Qilin Wu, S. E. Morin, and T. W. Mossberg, “Realization of a continuous-wave, two-photon optical laser,” *Phys. Rev. Lett.* **68**, 464–467 (1992).

[50] S. Stufler, P. Machnikowski, P. Ester, M. Bichler, V. M. Axt, T. Kuhn, and A. Zrenner, “Two-photon Rabi oscillations in a single  $In_xGa_{1-x}As/GaAs$  quantum dot,” *Phys. Rev. B* **73**, 125304 (2006).

[51] Elena del Valle, Stefano Zippilli, Fabrice P. Laussy, Alejandro Gonzalez-Tudela, Giovanna Morigi, and Carlos Tejedor, “Two-photon lasing by a single quantum dot in a high- $q$  microcavity,” *Phys. Rev. B* **81**, 035302 (2010).

[52] S. Felicetti, D. Z. Rossatto, E. Rico, E. Solano, and P. Forn-Díaz, “Two-photon quantum Rabi model with superconducting circuits,” *Phys. Rev. A* **97**, 013851 (2018).

[53] Alba Crescente, Matteo Carrega, Maura Sassetto, and Dario Ferraro, “Ultrafast charging in a two-photon Dicke quantum battery,” *Phys. Rev. B* **102**, 245407 (2020).

[54] Lu Wang, Shu-Qian Liu, Feng-lin Wu, Hao Fan, and Si-Yuan Liu, “Deep strong charging in a multiphoton anisotropic Dicke quantum battery,” *Phys. Rev. A* **110**, 042419 (2024).

[55] G. S. Agarwal, “Vacuum-field Rabi oscillations of atoms in a cavity,” *J. Opt. Soc. Am. B* **2**, 480–485 (1985).

[56] P. Alsing and M. S. Zubairy, “Collapse and revivals in a two-photon absorption process,” *J. Opt. Soc. Am. B* **4**, 177–184 (1987).

[57] R. R. Puri and R. K. Bullough, “Quantum electrodynamics of an atom making two-photon transitions in an ideal cavity,” *J. Opt. Soc. Am. B* **5**, 2021–2028 (1988).

[58] A. H. Toor and M. S. Zubairy, “Validity of the effective Hamiltonian in the two-photon atom-field interaction,” *Phys. Rev. A* **45**, 4951–4959 (1992).

[59] R. R. Puri and G. S. Agarwal, “Coherent two-photon transitions in Rydberg atoms in a cavity with finite  $Q$ ,” *Phys. Rev. A* **37**, 3879–3883 (1988).

[60] S. Felicetti, J. S. Pedernales, I. L. Egusquiza, G. Romero,

L. Lamata, D. Braak, and E. Solano, "Spectral collapse via two-phonon interactions in trapped ions," *Phys. Rev. A* **92**, 033817 (2015).

[61] Liwei Duan, You-Fei Xie, Daniel Braak, and Qing-Hu Chen, "Two-photon Rabi model: analytic solutions and spectral collapse," *J. Phys. A: Math. Theor.* **49**, 464002 (2016).

[62] R. J. Armenta Rico, F. H. Maldonado-Villamizar, and B. M. Rodriguez-Lara, "Spectral collapse in the two-photon quantum Rabi model," *Phys. Rev. A* **101**, 063825 (2020).

[63] C. F. Lo, "Spectral collapse in multiqubit two-photon Rabi model," *Sci. Rep.* **11**, 5409 (2021).

[64] Christopher C. Gerry and James B. Togeas, "Squeezing and photon antibunching from a two-photon Dicke model," *Optics Communications* **69**, 263–266 (1989).

[65] Jie Peng, Chenxiong Zheng, Guangjie Guo, Xiaoyong Guo, Xin Zhang, Chaosheng Deng, Guoxing Ju, Zhongzhou Ren, Lucas Lamata, and Enrique Solano, "Dark-like states for the multi-qubit and multi-photon Rabi models," *J. Phys. A: Math. Theor.* **50**, 174003 (2017).

[66] Shangyun Wang, Songbai Chen, and Jiliang Jing, "Effect of system energy on quantum signatures of chaos in the two-photon Dicke model," *Phys. Rev. E* **100**, 022207 (2019).

[67] Priyankar Banerjee, Deepti Sharma, and Aranya B. Bhattacherjee, "Enhanced photon squeezing in two-photon Dicke model," *Phys. Lett. A* **446**, 128287 (2022).

[68] Fabrizio Ramírez, David Villaseñor, Viani S. Morales-Guzmán, Darly Y. Castro, and Jorge G. Hirsch, "Loss of integrability in a system with two-photon interactions," *Phys. Rev. A* **112**, 063707 (2025).

[69] L. Garbe, I. L. Egusquiza, E. Solano, C. Ciuti, T. Coudreau, P. Milman, and S. Felicetti, "Superradiant phase transition in the ultrastrong-coupling regime of the two-photon Dicke model," *Phys. Rev. A* **95**, 053854 (2017).

[70] Xiang-You Chen and Yu-Yu Zhang, "Finite-size scaling analysis in the two-photon Dicke model," *Phys. Rev. A* **97**, 053821 (2018).

[71] Louis Garbe, Peregrine Wade, Fabrizio Minganti, Nathan Shammah, Simone Felicetti, and Franco Nori, "Dissipation-induced bistability in the two-photon Dicke model," *Sci. Rep.* **10**, 13408 (2020).

[72] Aanal Jayesh Shah, Peter Kirton, Simone Felicetti, and Hadiseh Alaeian, "Dissipative phase transition in the two-photon Dicke model," *Phys. Rev. Lett.* **135**, 173602 (2025).

[73] Cui-Lu Zhai, Wei Wu, Chun-Wang Wu, and Ping-Xing Chen, "Stark-induced tunable phase transition in the two-photon Dicke-Stark model," *Phys. Rev. A* **112**, 013720 (2025).

[74] (See the Supplemental Material at [...] for additional information about the two-photon Dicke model. This Supplemental Material includes Refs. [75–80]).

[75] M.A.M de Aguiar, K Furuya, C.H Lewenkopf, and M.C Nemes, "Chaos in a spin-boson system: Classical analysis," *Annals of Physics* **216**, 291–312 (1992).

[76] L. Bakemeier, A. Alvermann, and H. Fehske, "Dynamics of the Dicke model close to the classical limit," *Phys. Rev. A* **88**, 043835 (2013).

[77] M. A. Bastarrachea-Magnani, S. Lerma-Hernández, and J. G. Hirsch, "Comparative quantum and semiclassical analysis of atom-field systems. I. Density of states and excited-state quantum phase transitions," *Phys. Rev. A* **89**, 032101 (2014).

[78] M. A. Bastarrachea-Magnani, S. Lerma-Hernández, and J. G. Hirsch, "Comparative quantum and semiclassical analysis of atom-field systems. II. Chaos and regularity," *Phys. Rev. A* **89**, 032102 (2014).

[79] Miguel Angel Bastarrachea-Magnani, Baldemar López del Carpio, Sergio Lerma-Hernández, and Jorge G Hirsch, "Chaos in the Dicke model: Quantum and semiclassical analysis," *Phys. Scr.* **90**, 068015 (2015).

[80] J. Chávez-Carlos, M. A. Bastarrachea-Magnani, S. Lerma-Hernández, and J. G. Hirsch, "Classical chaos in atom-field systems," *Phys. Rev. E* **94**, 022209 (2016).

## Supplemental Material: The superradiant phase is a finite size effect in two-photon processes

Fabrizio Ramírez,<sup>1</sup> David Villaseñor,<sup>2</sup> Nahum Vázquez,<sup>1</sup> and Jorge G. Hirsch<sup>1</sup>

<sup>1</sup>*Instituto de Ciencias Nucleares, Universidad Nacional Autónoma de México,  
Apdo. Postal 70-543, C.P. 04510 Mexico City, Mexico*

<sup>2</sup>*CAMTP - Center for Applied Mathematics and Theoretical Physics,  
University of Maribor, Mladinska 3, SI-2000 Maribor, Slovenia, European Union*

This Supplemental Material provides additional information on the two-photon Dicke model. In Sec. , we review the Holstein-Primakoff and Bogoliubov transformations, which lead to an analytical expression for the ground-state energy in both the normal and superradiant phases of the system. In Sec. , we introduce the mean-field approximation using squeezed vacuum states, providing a classical limit for the system. The extreme values of the equations of motion derived from this classical limit yield analytic expressions for the ground-state energy, the number of photons, and atomic inversion in both the normal and superradiant phases. In Sec. , we perform a similar derivation using coherent states. Finally, in Sec. , we present further evidence regarding the disappearance of the superradiant phase, including the case of null atomic frequency.

### HOLSTEIN-PRIMAKOFF AND BOGOLIUBOV TRANSFORMATIONS

Following the procedure introduced in Ref. [69], we employ a Holstein-Primakoff transformation in the two-photon Dicke Hamiltonian  $\hat{H}_D$ , given in Eq. (1) of the main text, to change the collective atomic operators into bosonic operators

$$\hat{J}_z = \hat{b}^\dagger \hat{b} - j, \quad \hat{J}_+ = \hat{b}^\dagger \sqrt{2j - \hat{b}^\dagger \hat{b}}, \quad \hat{J}_- = \sqrt{2j - \hat{b}^\dagger \hat{b}} \hat{b}, \quad (S1)$$

and displace them with their mean value in the ground state  $|E_0\rangle$

$$\hat{b} = \hat{d} + \langle E_0 | \hat{b} | E_0 \rangle, \quad \langle E_0 | \hat{b} | E_0 \rangle = \langle E_0 | \hat{b}^\dagger | E_0 \rangle^* = \sqrt{j} b, \quad \langle E_0 | \hat{b}^\dagger \hat{b} | E_0 \rangle = j |b|^2, \quad (S2)$$

where  $b \in \mathbb{C}$  is a variational parameter and  $[\hat{b}, \hat{b}^\dagger] = [\hat{d}, \hat{d}^\dagger] = \hat{\mathbb{I}}$ . Neglecting the high order terms of the operator  $\hat{d}$ , we get

$$\hat{H}_D = \omega \hat{a}^\dagger \hat{a} + \frac{\gamma(b^* + b)}{2} \sqrt{2 - |b|^2} \left( \hat{a}^{\dagger 2} + \hat{a}^2 \right) + j\omega_0 \left( |b|^2 - 1 \right). \quad (S3)$$

The last Hamiltonian can be diagonalized using a Bogoliubov transformation

$$\hat{a} = u \hat{c} - v \hat{c}^\dagger, \quad \hat{a}^\dagger = u^* \hat{c}^\dagger - v^* \hat{c} \quad (S4)$$

where  $u = u^* = \cosh(r)$ ,  $v = v^* = \sinh(r)$ , and  $[\hat{a}, \hat{a}^\dagger] = [\hat{c}, \hat{c}^\dagger] = \hat{\mathbb{I}}$ . The new Hamiltonian is given by

$$\hat{H}_D = A \hat{c}^\dagger \hat{c} + B \left( \hat{c}^{\dagger 2} + \hat{c}^2 \right) + C, \quad (S5)$$

where

$$A = \omega \left( u^2 + v^2 \right) - 2\gamma(b^* + b) \sqrt{2 - |b|^2} uv, \quad (S6)$$

$$B = \frac{\gamma(b^* + b)}{2} \sqrt{2 - |b|^2} \left( u^2 + v^2 \right) - \omega uv, \quad (S7)$$

$$C = \omega v^2 - \gamma(b^* + b) \sqrt{2 - |b|^2} uv + j\omega_0 \left( |b|^2 - 1 \right). \quad (S8)$$

Considering  $B = 0$ , we arrive at the solution

$$\hat{H}_D = 2 \left[ E_0 + \frac{\omega}{2} - j\omega_0 \left( |b|^2 - 1 \right) \right] \hat{c}^\dagger \hat{c} + E_0, \quad (S9)$$

where

$$E_0 = \frac{\cosh(2r_b)}{2\omega} \left[ \omega^2 - \gamma^2 (b^* + b)^2 \left( 2 - |b|^2 \right) \right] + j\omega_0 \left( |b|^2 - 1 \right) - \frac{\omega}{2}, \quad (\text{S10})$$

is the ground-state energy and

$$r_b = \frac{1}{2} \operatorname{arctanh} \left( \frac{\gamma(b^* + b)}{\omega} \sqrt{2 - |b|^2} \right) \quad (\text{S11})$$

is the squeezing parameter of the ground state  $|E_0\rangle = |r_b\rangle = e^{(r_b^* a^2 - r_b a^{\dagger 2})/2} |0\rangle$ , which fulfills  $\langle E_0 | \hat{a} | E_0 \rangle = \langle E_0 | \hat{a}^\dagger | E_0 \rangle = 0$ ,  $\langle E_0 | \hat{a}^2 | E_0 \rangle = \langle E_0 | \hat{a}^{\dagger 2} | E_0 \rangle^* = -\sinh(r_b) \cosh(r_b)$ , and  $\langle E_0 | \hat{a}^\dagger \hat{a} | E_0 \rangle = \sinh^2(r_b)$ .

The minimization of the ground-state energy  $E_0$  with respect to the variational parameter  $b$  gives the extreme values for each of the normal and superradiant phases

$$b_0 = b_0^* = \begin{cases} 0 & \text{for (NP)} \\ \pm \left( 1 - \frac{j\omega_0\omega}{2\gamma^2} \sqrt{\frac{1 - \frac{4\gamma^2}{\omega^2}}{1 - \frac{j^2\omega_0^2}{\gamma^2}}} \right)^{1/2} & \text{for (SP)} \end{cases} \quad (\text{S12})$$

Substituting the previous extreme values in Eq. (S10), we recover Eq. (5) in the main text.

### MEAN-FIELD APPROXIMATION WITH SQUEEZED VACUUM STATES

Inspired in the previous results of the ground state of the two-photon Dicke Hamiltonian, we introduce a mean-field approximation to define a classical phase space using squeezed vacuum states  $|\xi\rangle$  for the bosonic sector

$$|\xi\rangle = e^{(\xi^* \hat{a}^2 - \xi \hat{a}^{\dagger 2})/2} |0\rangle, \quad (\text{S13})$$

and Bloch coherent states  $|\beta\rangle$  for the atomic sector

$$|\beta\rangle = \frac{1}{(1 + |\beta|^2)^j} e^{\beta \hat{J}_+} |j, -j\rangle \quad (\text{S14})$$

with complex parameter

$$\beta = \frac{Q + iP}{\sqrt{4 - Q^2 - P^2}}, \quad (\text{S15})$$

where  $(Q, P)$  are the atomic classical variables of phase space. In the above expressions,  $|0\rangle$  is the bosonic vacuum state and  $|j, -j\rangle$  is the atomic state with all atoms in the ground state. The squeezing parameter  $\xi = re^{i\theta}$  provides a connection with bosonic classical variables  $(q, p)$  using the transformation  $q = \sqrt{2/j} \sinh(r) \cos(\theta)$  and  $p = \sqrt{2/j} \sinh(r) \sin(\theta)$

$$\langle \xi | \hat{a} | \xi \rangle = \langle \xi | \hat{a}^\dagger | \xi \rangle = 0, \quad (\text{S16})$$

$$\langle \xi | \hat{a}^2 | \xi \rangle = \langle \xi | \hat{a}^{\dagger 2} | \xi \rangle^* = -e^{i\theta} \sinh(r) \cosh(r) = -\sqrt{\frac{j}{2} \left( 1 + \frac{j}{2} (q^2 + p^2) \right)} (q + ip), \quad (\text{S17})$$

$$\langle \xi | \hat{a}^\dagger \hat{a} | \xi \rangle = \sinh^2(r) = \frac{j}{2} (q^2 + p^2). \quad (\text{S18})$$

The expectation value of the quantum Hamiltonian  $\hat{H}_D$  [Eq. (1) in the main text] under squeezed vacuum states

$|\mathbf{x}\rangle \equiv |\xi\rangle \otimes |\beta\rangle$ , where  $\mathbf{x} = (q, p; Q, P)$ , provides a classical limit of the two-photon Dicke model

$$\begin{aligned} h_D(\mathbf{x}) &= \frac{1}{j} \langle \mathbf{x} | \hat{H}_D | \mathbf{x} \rangle = \frac{1}{j} \langle \beta | \otimes \langle \xi | \hat{H}_D | \xi \rangle \otimes | \beta \rangle \\ &= \frac{1}{j} \left\{ \omega \langle \xi | \hat{a}^\dagger \hat{a} | \xi \rangle - j\omega_0 \frac{1 - |\beta|^2}{1 + |\beta|^2} + \gamma \left[ \langle \xi | \hat{a}^{\dagger 2} | \xi \rangle + \langle \xi | \hat{a}^2 | \xi \rangle \right] \frac{\beta + \beta^*}{1 + |\beta|^2} \right\} \\ &= \frac{1}{j} \left\{ \omega \sinh^2(r) + j\omega_0 \left( \frac{Q^2 + P^2}{2} - 1 \right) - 2\gamma \sinh(r) \cosh(r) \cos(\theta) Q \sqrt{1 - \frac{Q^2 + P^2}{4}} \right\} \\ &= \frac{\omega}{2} (q^2 + p^2) + \omega_0 \left( \frac{Q^2 + P^2}{2} - 1 \right) - 2\gamma q Q \sqrt{\left( \frac{1}{2j} + \frac{q^2 + p^2}{4} \right) \left( 1 - \frac{Q^2 + P^2}{4} \right)}, \end{aligned} \quad (\text{S19})$$

where the energy shells  $\epsilon = E/j$  are scaled to the system size  $j$ .

The Hamilton equations of motion of the Hamiltonian presented in Eq. (S19) are given by

$$\dot{q} = \frac{\partial h_D(\mathbf{x})}{\partial p} = \omega p - \frac{\gamma q p Q}{2} \sqrt{1 - \frac{Q^2 + P^2}{4}} \left( \frac{1}{2j} + \frac{q^2 + p^2}{4} \right)^{-1/2}, \quad (\text{S20})$$

$$\dot{p} = -\frac{\partial h_D(\mathbf{x})}{\partial q} = -\omega q + 2\gamma Q \sqrt{1 - \frac{Q^2 + P^2}{4}} \left( \frac{1}{2j} + \frac{2q^2 + p^2}{4} \right) \left( \frac{1}{2j} + \frac{q^2 + p^2}{4} \right)^{-1/2}, \quad (\text{S21})$$

$$\dot{Q} = \frac{\partial h_D(\mathbf{x})}{\partial P} = \omega_0 P + \frac{\gamma q Q P}{2} \sqrt{\frac{1}{2j} + \frac{q^2 + p^2}{4}} \left( 1 - \frac{Q^2 + P^2}{2} \right)^{-1/2}, \quad (\text{S22})$$

$$\dot{P} = -\frac{\partial h_D(\mathbf{x})}{\partial Q} = -\omega_0 Q + 2\gamma q \sqrt{\frac{1}{2j} + \frac{q^2 + p^2}{4}} \left( 1 - \frac{2Q^2 + P^2}{4} \right) \left( 1 - \frac{Q^2 + P^2}{4} \right)^{-1/2}. \quad (\text{S23})$$

The minimization of the last set of equations  $\dot{q} = \dot{p} = \dot{Q} = \dot{P} = 0$  provides the extreme values

$$\mathbf{x}_0 = (0, 0; 0, 0), \quad (\text{S24})$$

$$\mathbf{x}_+ = \left( \pm \frac{1}{\sqrt{j}} \left( \sqrt{\frac{1 - \frac{4\gamma^2}{\omega^2}}{1 - \frac{j^2\omega_0^2}{\gamma^2}}} - 1 \right)^{1/2}, 0; + \left( 2 - \frac{j\omega_0\omega}{\gamma^2} \sqrt{\frac{1 - \frac{4\gamma^2}{\omega^2}}{1 - \frac{j^2\omega_0^2}{\gamma^2}}} \right)^{1/2}, 0 \right), \quad (\text{S25})$$

$$\mathbf{x}_- = \left( \pm \frac{1}{\sqrt{j}} \left( \sqrt{\frac{1 - \frac{4\gamma^2}{\omega^2}}{1 - \frac{j^2\omega_0^2}{\gamma^2}}} - 1 \right)^{1/2}, 0; - \left( 2 - \frac{j\omega_0\omega}{\gamma^2} \sqrt{\frac{1 - \frac{4\gamma^2}{\omega^2}}{1 - \frac{j^2\omega_0^2}{\gamma^2}}} \right)^{1/2}, 0 \right), \quad (\text{S26})$$

where the solutions  $\mathbf{x}_\pm$  explicitly depend on the system size  $j$ .

Evaluating the Hamiltonian of Eq. (S19) with the extreme values  $\mathbf{x}_m = \mathbf{x}_{0,\pm}$  [Eqs. (S24)-(S26)], we find the ground-state energy  $E_0 = j h_D(\mathbf{x}_m)$  presented in Eq. (5) in the main text. The last result agrees with the description of the Holstein-Primakoff transformation presented in Sec. . Moreover, the expectation values of operators  $\hat{a}^\dagger \hat{a}$  and  $\hat{J}_z$  under the squeezed vacuum states provide the expressions

$$\langle \mathbf{x} | \hat{a}^\dagger \hat{a} | \mathbf{x} \rangle = \langle \beta | \otimes \langle \xi | \hat{a}^\dagger \hat{a} | \xi \rangle \otimes | \beta \rangle = \frac{j}{2} (q^2 + p^2), \quad (\text{S27})$$

$$\frac{\langle \mathbf{x} | \hat{J}_z | \mathbf{x} \rangle}{j} = \frac{1}{j} \langle \beta | \otimes \langle \xi | \hat{J}_z | \xi \rangle \otimes | \beta \rangle = \frac{Q^2 + P^2}{2} - 1. \quad (\text{S28})$$

Evaluating the last expressions with the extreme values  $\mathbf{x}_m$ , we find the corresponding Eq. (6) and Eq. (7) in the main text.

## MEAN-FIELD APPROXIMATION WITH COHERENT STATES

Usual mean-field approximations for spin-boson systems consider coherent states as trial states [75–80]. We consider Glauber coherent states  $|\alpha\rangle$  to describe the bosonic sector

$$|\alpha\rangle = e^{-|\alpha|^2/2} e^{\alpha \hat{a}^\dagger} |0\rangle, \quad (\text{S29})$$

with complex parameter

$$\alpha = \sqrt{\frac{j}{2}}(q + ip), \quad (\text{S30})$$

and Bloch coherent states  $|\beta\rangle$  to describe the atomic sector [Eq. (S14) and Eq. (S15)].

The expectation value of the quantum Hamiltonian  $\hat{H}_D$  [Eq. (1) in the main text] under Glauber-Bloch coherent states  $|\mathbf{y}\rangle \equiv |\alpha\rangle \otimes |\beta\rangle$ , where  $\mathbf{y} = (q, p; Q, P)$ , provides a classical limit of the two-photon Dicke model [68]

$$\begin{aligned} h_D(\mathbf{y}) &= \frac{1}{j} \langle \mathbf{y} | \hat{H}_D | \mathbf{y} \rangle = \frac{1}{j} \langle \beta | \otimes \langle \alpha | \hat{H}_D | \alpha \rangle \otimes | \beta \rangle \\ &= \frac{1}{j} \left\{ \omega |\alpha|^2 - j\omega_0 \frac{1 - |\beta|^2}{1 + |\beta|^2} + \gamma \left[ (\alpha^*)^2 + \alpha^2 \right] \frac{\beta + \beta^*}{1 + |\beta|^2} \right\} \\ &= \frac{\omega}{2} (q^2 + p^2) + \omega_0 \left( \frac{Q^2 + P^2}{2} - 1 \right) + \gamma (q^2 - p^2) Q \sqrt{1 - \frac{Q^2 + P^2}{4}}. \end{aligned} \quad (\text{S31})$$

The Hamilton equations of motion of the Hamiltonian presented in Eq. (S31) are described by

$$\dot{q} = \frac{\partial h_D(\mathbf{y})}{\partial p} = \omega p - 2\gamma p Q \sqrt{1 - \frac{Q^2 + P^2}{4}}, \quad (\text{S32})$$

$$\dot{p} = -\frac{\partial h_D(\mathbf{y})}{\partial q} = -\omega q - 2\gamma q Q \sqrt{1 - \frac{Q^2 + P^2}{4}}, \quad (\text{S33})$$

$$\dot{Q} = \frac{\partial h_D(\mathbf{y})}{\partial P} = \omega_0 P - \frac{\gamma (q^2 - p^2) Q P}{4} \left( 1 - \frac{Q^2 + P^2}{4} \right)^{-1/2}, \quad (\text{S34})$$

$$\dot{P} = -\frac{\partial h_D(\mathbf{y})}{\partial Q} = -\omega_0 Q - \gamma (q^2 - p^2) \left( 1 - \frac{2Q^2 + P^2}{4} \right) \left( 1 - \frac{Q^2 + P^2}{4} \right)^{-1/2}. \quad (\text{S35})$$

The minimization of the last set of equations  $\dot{q} = \dot{p} = \dot{Q} = \dot{P} = 0$  provides the extreme values

$$\mathbf{y}_0 = (0, 0; 0, 0), \quad (\text{S36})$$

$$\mathbf{y}_+ = \left( \pm(-1)^{1/4} \sqrt{\frac{\omega_0}{\gamma}} \left( 1 - \frac{4\gamma^2}{\omega^2} \right)^{-1/4}, 0; + \left( 2 + i \frac{\omega}{\gamma} \sqrt{1 - \frac{4\gamma^2}{\omega^2}} \right)^{1/2}, 0 \right), \quad (\text{S37})$$

$$\mathbf{y}_- = \left( \pm(-1)^{1/4} \sqrt{\frac{\omega_0}{\gamma}} \left( 1 - \frac{4\gamma^2}{\omega^2} \right)^{-1/4}, 0; - \left( 2 + i \frac{\omega}{\gamma} \sqrt{1 - \frac{4\gamma^2}{\omega^2}} \right)^{1/2}, 0 \right), \quad (\text{S38})$$

where  $\mathbf{y}_0 \in \mathbb{R}$  and  $\mathbf{y}_\pm \in \mathbb{C}$ . The real extreme value  $\mathbf{y}_0$  is the only allowed solution that reproduces the ground-state energy of the normal phase, when we evaluate  $h_D(\mathbf{y}_0) = E_0/j$ .

Now, if we consider the solutions obtained with squeezed states [Eqs. (S24)-(S26)] and take the thermodynamic limit  $j \rightarrow \infty$ , we arrive to the solutions obtained with coherent states

$$\lim_{j \rightarrow \infty} \mathbf{x}_{0,\pm} = \mathbf{y}_{0,\pm}. \quad (\text{S39})$$

The last expression shows that the solutions  $\mathbf{x}_\pm$  [Eqs. (S25)-(S26)] associated to superradiance become complex in the thermodynamic limit and coincide with  $\mathbf{y}_\pm$  [Eqs. (S37)-(S38)]. As a result, the superradiant phase is not allowed.

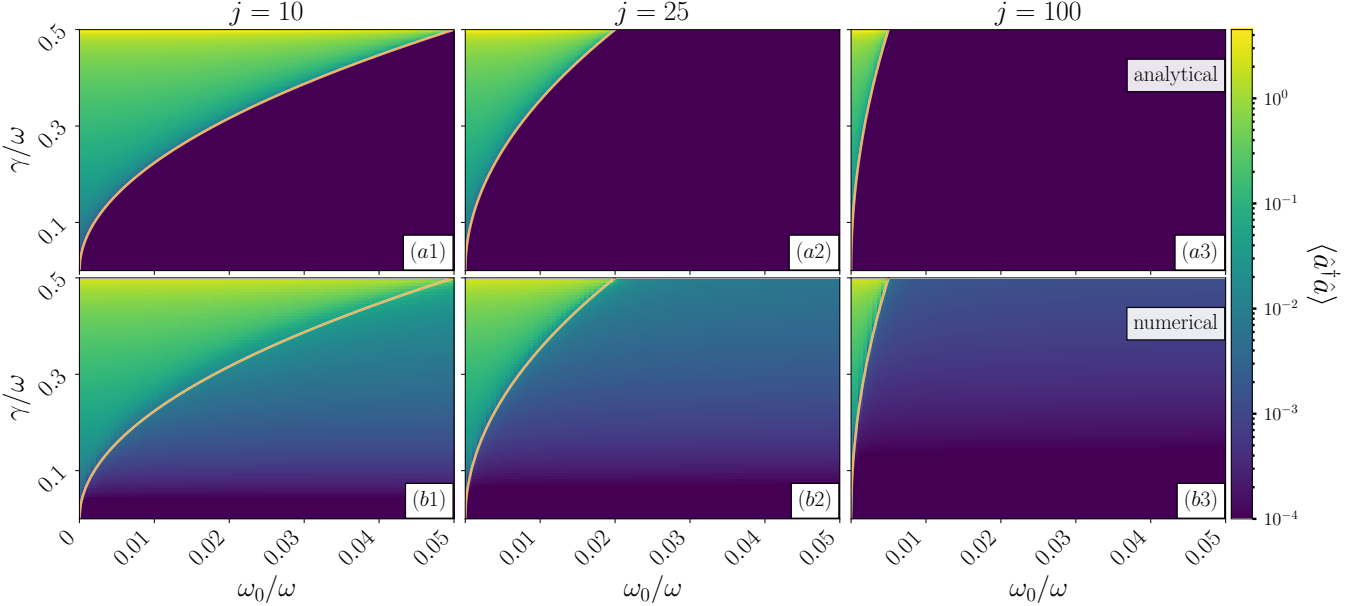


FIG. S1. (a1)-(a3) Phase diagrams of the number of photons  $\langle \hat{a}^\dagger \hat{a} \rangle$  [Eq. (6) in the main text] as a function of the scaled atomic frequency  $\omega_0/\omega$  and the scaled coupling parameter  $\gamma/\omega$ . The color scheme represents the value of the number of photons in a logarithmic scale. The orange solid line represents the scaled critical coupling  $\gamma_c/\omega = \sqrt{\omega_0 j / (2\omega)}$ . (b1)-(b3) Numerical implementations of panels (a1)-(a3). Each column identifies a different system size: (a1)-(b1)  $j = 10$ , (a2)-(b2)  $j = 25$ , and (a3)-(b3)  $j = 100$ .

#### DISAPPEARANCE OF THE SUPERRADIANT PHASE AND CASE WITH NULL ATOMIC FREQUENCY

We show further evidence of the disappearance of the superradiant phase in the two-photon Dicke model. Similar to the phase diagrams presented in the main text for the normalized atomic excitation, we present phase diagrams for the number of photons and the ground-state energy.

In Fig. S1, we show phase diagrams of the number of photons  $\langle \hat{a}^\dagger \hat{a} \rangle$  [Eq. (6) in the main text] as a function of the scaled atomic frequency  $\omega_0/\omega$  and the scaled coupling parameter  $\gamma/\omega$ . The first row [Figs. S1(a1)-S1(a3)] shows the number of photons for three values of the system size  $j$  that increase from left to right. The color scheme represents the value of the number of photons in a logarithmic scale for the sake of clarity. The second row [Figs. S1(b1)-S1(b3)] shows the numerical implementation, where we see how the numerical noise is more evident when compared with the analytical results. In general, we again identify how the superradiant phase shrinks with increasing system size  $j$ .

Similar phase diagrams are presented in Fig. S2 for the ground-state energy  $E_0$  [Eq. (5) in the main text]. The ground-state energy was displaced by adding the value of the ground-state energy of the normal phase,  $E_0 + j|\omega_0|$ . The first row [Figs. S2(a1)-S2(a3)] and the second row [Figs. S2(b1)-S2(b3)] identify the analytical and numerical implementations, respectively. The color scheme represents the value of the displaced ground-state energy. The figures confirm again that the superradiant phase vanishes by increasing the system size  $j$ .

When  $\omega_0 = 0$ , all the observables presented in Eqs. (5)-(7) of the main text become independent of the system size  $j$ . In Fig. S3, we display these observables as a function of the scaled coupling parameter  $\gamma/\omega$ . We illustrate the ground-state energy in Fig. S3(a), which has been displaced by the ground-state energy of the normal phase  $E_0 + j|\omega_0|$ . In Fig. S3(b), we present the number of photons  $\langle \hat{a}^\dagger \hat{a} \rangle$ . Finally, in Fig. S3(c), we show the atomic inversion  $\langle \hat{J}_z \rangle / j$ . The red dashed line indicates the spectral collapse at  $\gamma/\omega = 0.5$ . In Fig. S3(a), we observe a finite value of the displaced ground-state energy when the spectral collapse occurs. Figure S3(b) shows a divergence in the number of photons at the point of spectral collapse, while in Fig. S3(c), we find that the atomic inversion has a constant mean value of zero, as expected. Notice that in this case the atomic degree of freedom becomes decoupled from the photonic one. The divergence in the photon number is a result of spectral collapse; it is independent of the number of photons and is not related to a superradiant phase.

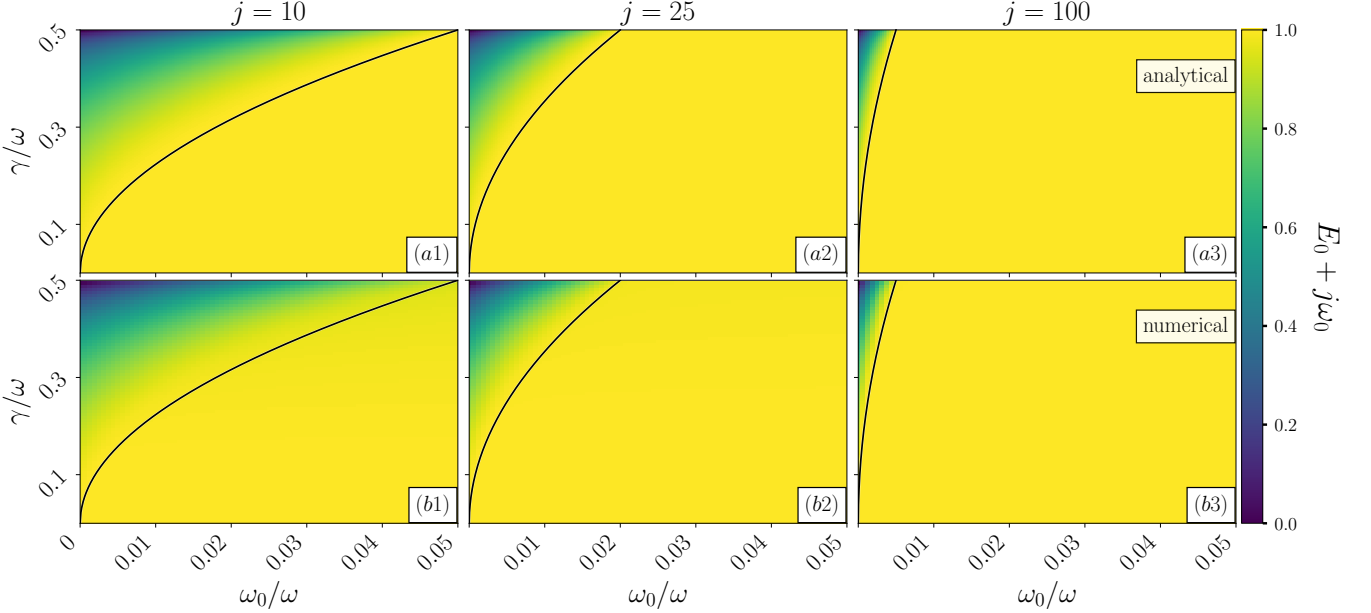


FIG. S2. (a1)-(a3) Phase diagrams of the displaced ground-state energy  $E_0 + j|\omega_0|$  [Eq. (5) in the main text] as a function of the scaled atomic frequency  $\omega_0/\omega$  and the scaled coupling parameter  $\gamma/\omega$ . The color scheme represents the value of the displaced ground-state energy. The black solid line represents the scaled critical coupling  $\gamma_c/\omega = \sqrt{\omega_0 j/(2\omega)}$ . (b1)-(b3) Numerical implementations of panels (a1)-(a3). Each column identifies a different system size: (a1)-(b1)  $j = 10$ , (a2)-(b2)  $j = 25$ , and (a3)-(b3)  $j = 100$ .

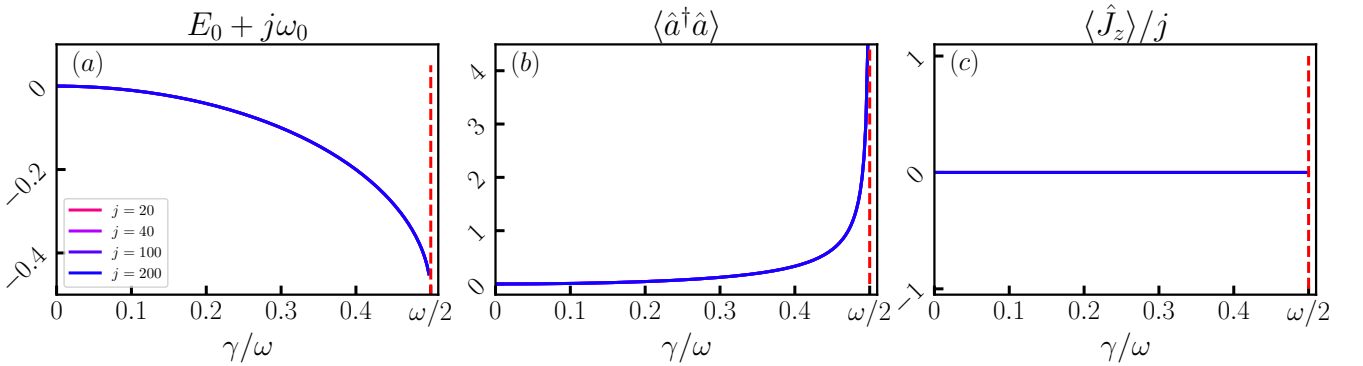


FIG. S3. Projections of (a) the displaced ground-state energy  $E_0 + j|\omega_0|$  [Eq. (5) in the main text], (b) the number of photons  $\langle \hat{a}^\dagger \hat{a} \rangle$  [Eq. (6) in the main text], and (c) the atomic inversion  $\langle \hat{J}_z \rangle/j$  [Eq. (7) in the main text] as a function of the scaled coupling parameter  $\gamma/\omega$ . The vertical red dashed line represents the spectral collapse at  $\gamma/\omega = 0.5$ . The atomic frequency is  $\omega_0/\omega = 0$ .